Behaviour of polyhedra in Sr_2NiMoO_6 at high pressure and temperature

C L Bull, C J Ridley, N P Funnell and K S Knight

Published version information

Citation: C Bull et al. "Behaviour of polyhedra in Sr_2NiMoO_6 at high pressure and temperature." Journal of Solid State Chemistry, vol. 290 (2020): 121474.

DOI: 10.1016/j.jssc.2020.121474

Behaviour of Polyhedra in Sr_2NiMoO_6 at High Pressure and Temperature

C L Bull[a], C J Ridley[a], N P Funnell[a] and K S Knight[b,c]

[a]ISIS Neutron and Muon Facility, STFC, Rutherford Appleton Laboratory, Chilton, OXON, OX11 0QX, U.K.
[b]Department of Earth Sciences, University College London, Gower Street, London, WC1E 6BT, U.K.
[c]Department of Earth Sciences, The Natural History Museum, Cromwell Road, London, SW7 5BD, U.K.

ARTICLE INFO

Keywords:
Sr_2NiMoO_6
high-pressure
neutron diffraction
octahedral tilting
perovskite
high-temperature

ABSTRACT

The high-pressure behaviour of Sr_2NiMoO_6 has been measured up to ∼6 GPa using neutron powder diffraction. With increasing pressure the tetragonal ($I4/m$) symmetry is maintained and the structure becomes more distorted. The distortion is a result of increased octahedral tilting away from the idealised cubic symmetry by rotation around the c-axis in the ab plane. The pressure equation of state has been determined and gives values of V_0=243.10(2) Å^3, B_0 =155(2) GPa and B'=3.1(6). We also report the high temperature behaviour at ambient pressure and observe a transition from tetragonal to cubic symmetry at ∼ 573 K.

1. Introduction

The aristotype perovskite structure is cubic with the general formula ABX_3, where A is typically a large electropositive cation, B a small transition metal or main group ion and X normally an oxide or halide ion. The A cation is found in the centre of 8 corner shared BX_6 octahedra. By chemically modifying the contents of the A, B and X sites it is possible to produce a wide variety of materials. However, by changing the size of the A, B and X ionic radii the material may not crystallise in the aristotype cubic structure but instead concerted rotations of the BX_6 octahedra may result in lowering of the crystallographic symmetry, the degree of which are dependent on the relative ionic radii.[1] Doubling of the perovskite structure to give $A_2BB'X_6$ (where the prime indicates a different ion) can give rise to an ordered arrangement of the cations in a wide range of symmetries, for example, tetragonal Ca_2CrTaO_6 and cubic Ba_2MnWO_6.[2, 3]

$SrNiO_3$ is a hexagonal perovskite (in which the octahedra are face sharing not corner sharing as in the aristotype perovskite structure) and is a half metallic ferroelectric and finds applications in spintronics as a spin injector material with the Ni in the +4 oxidation state. [4] The cubic perovskite $SrMoO_3$ is metallic (with the Mo in a +4 oxidation state) and Pauli paramagnetic down to low temperatures and is a possible candidate for use as a transparent conductive oxide coating, which has a wide variety of applications including use in solar cells.[5, 6, 7] Given the diverse structure and properties of these two materials it is of interest to see what properties the material possesses when the double perovskite is made from the two different B-site cations.

Sr_2NiMoO_6 crystallises with rock salt ordering of the B-site cations in the tetragonal space group $I4/m$ (Glazer tilt system = $a^0a^0c^-$ [8]) and no change in symmetry is observed down to 20 K.[9] Previous studies have suggested a range of tetragonal unit cells including $a \approx 3.9237$ and $c \approx 3.9474$ [10], $a \approx 7.90$ and $c \approx 7.84$ [11, 12] and $a \approx 5.55$ and $c \approx 7.89$ Å.[13, 14] Gunjikar *et al* reported an anomaly in the heat capacity measurements at 452 K, suggesting a possible structural transition.[15] Other structural studies report a transition from tetragonal to cubic symmetry at higher temperatures and yet see no anomaly in the diffraction pattern around 452 K. The structural transition from the tetragonal phase to a cubic phase ($Fm\bar{3}m$, $a^0a^0a^0$ tilt system) is reported in the temperature range 503–550 K,[16, 11, 9] and the discrepancies in transition temperature are suggested to be a result of differences in cation ordering or synthesis conditions.[16] Sr_2NiMoO_6 is an antiferromagnetic material with a Néel temperature of 80 K [9] where Sr is found in the +2 oxidation state, the Ni in +2 and Mo in a +6 oxidation state, and it is this large difference in the B site charge that results in the rock salt ordering. The material finds a potential application in chemical looping combustion as a result of its oxygen transfer properties.[17, 18]

The application of high pressure to double perovskite materials is well known to induce structural phase transitions for example, the monoclinic to rhombohedral transition in La_2NiMnO_6[19] and the pseudo-cubic to tetragonal transition in Sr_2CrReO_6[20]. In contrast some systems, such as Sr_2FeOsO_6, remain structurally stable, despite pressure-induced magnetic transitions.[21]

There is one reported high pressure structural study of Sr_2NiMoO_6.[16] This energy dispersive x-ray diffraction study reported 5 pressure points up to a pressure of 5.7 GPa. The study showed an increase in tetragonal strain with pressure, while peak broadening suggested a possible phase transition to lower symmetry.

In the current study we have reinvestigated the compressive behaviour of Sr_2NiMoO_6 up to pressure of 6 GPa. Using neutron powder diffraction, we show that there is no pressure-induced transformation to a lower symmetry structure. We present the compression behaviour of the individual polyhedra and individual bond lengths.

*Corresponding author
thumbnails/qas-email.jpeg (C.L. Bull)
ORCID(s): 0000-0002-5170-6674 (C.L. Bull); 0000-0002-3060-9656 (C.J. Ridley); 0000-0001-6280-036X (N.P. Funnell)

2. Experimental

2.1. Synthesis and Characterisation

Tetragonal Sr_2NiMoO_6 was prepared by mixing stoichiometric amounts of dried $SrCO_3$, NiO and MoO_3, in accordance with previous reports.[22] The ground mixture was pelletised and annealed at 1373 K for 24 hours and cooled slowly back to 293 K; the grinding, pelletising and annealing process was repeated until phase pure Sr_2NiMoO_6 resulted and confirmed to be single phase by x-ray diffraction. The final product was also characterised by neutron power diffraction using the POLARIS instrument at the ISIS Neutron and Muon Source, UK.[23]

2.2. High-Pressure Neutron Diffraction

High-pressure neutron-diffraction measurements were performed on the PEARL instrument at the ISIS Neutron and Muon Source, UK.[24] The sample was loaded into a TiZr null-scattering encapsulated gasket [25] and placed within single-toroidal profile anvils machined from zirconia toughened alumina. Lead was included in the sample chamber to act as a pressure marker and perdeuterated methanol:ethanol (4:1) was included as a hydrostatic pressure transmitting medium.[26] The gasket anvil assembly was placed in a V3 Paris-Edinburgh press and a sealing load of 6 tonnes was applied.[27] Time–of–flight (ToF) diffraction patterns were obtained in steps of ∼0.25 GPa steps up to a maximum of 6 GPa. Diffraction data were collected for ∼2 hours per pressure step. Data were focussed and corrected for anvil attenuation using in house software.[28] The resulting ToF diffraction patterns were analysed using the GSAS suite of programmes.[29] The equation of state and compressibilties were determined from the PASCal program.[30]

2.3. High Temperature X-ray Diffraction

High temperature x-ray diffraction measurements were obtained in 50 K steps from 298 K to 1375 K in an air atmosphere. A Rigaku Smartlab diffractometer (λ=1.540562 Å) equipped with an AntonParr hot stage, was used and diffraction patterns were measured in the range of 20–100° in 2θ with a step size of 0.01° and a collection time of 0.3 s per step.

3. Results & Discussion

Figure 1 shows the neutron diffraction pattern of Sr_2NiMoO_6 and associated Rietveld fit obtained from the high angle bank of the POLARIS instrument. The results of the Rietveld refinement are detailed in Table 1 and are in good agreement with those previously reported. There is a small < 1 weight % NiO contaminant phase present in the diffraction pattern. The diffraction pattern of Sr_2NiMoO_6, as loaded in the Paris–Edinburgh press, and associated Rietveld refinements are shown in Figure 1, and the results are detailed in Table 1. The tetragonal $I4/m$ space group allows the Ni and Mo to be located on specific crystallographic sites and not disordered on one crystallographic site. The Mo and Ni atoms sit on the $2a$ $(0,0,0)$ and $2b$ $(\frac{1}{2},\frac{1}{2},0)$ Wyckoff sites respectively, placing the alternative transition metal on the Wyckoff site of the other ion and refining site occupation results in 100% occupation of a specific transition metal and hence the sample is fully ordered. The Sr sits on the $4d$ $(0,\frac{1}{2},\frac{1}{4})$ Wyckoff sites and two O atoms sit on $4e$ and $8h$ positions with fractional co-ordinates of $(0,0,\frac{1}{4}+w_1)$ and $(\frac{1}{4}+u_2,\frac{1}{4}+v_2,0)$. The values w_1, u_2 and v_2 represent the distortion from the ideal cubic symmetry.

Table 1
Crystallographic structure and quality of fit information determined from Rietveld refinement of neutron diffraction data of Sr_2NiMoO_6 at ambient pressure and temperature. Notes: [a]measured from within recovered encapsulated TiZr gasket, following PEARL study. [b]Data from as loaded sample with applied load of 6 tonnes, [c]the values of wRp, Rp and χ^2 for the POLARIS data set are the figures of merit for the 52, 92 ands 147° detectors bank during simultaneous refinements.

Parameter	POLARIS[a]	PEARL[b]	Literature[9]
Spacegroup	$I4/m$	$I4/m$	$I4/m$
$a_{tet} = b_{tet}$ (Å)	5.5422(7)	5.54725(8)	5.5473(3)
c_{tet} (Å)	7.89112(11)	7.8946(2)	7.8970(3)
Volume (Å)^3	242.583(2)	242.932(9)	242.67(1)
O1 z	0.2431(4)	0.246(3)	0.2417(6)
O2 x	0.2174(3)	0.2213(4)	0.2158(4)
O2 z	0.2688(3)	0.2768(15)	0.2703(5)
Sr–O1 (Å)×4	2.77264(8)	2.77381(10)	2.774(1)
Sr–O2 (Å)×4	2.6434(7)	2.6494(15)	2.634(2)
Sr–O2 (Å)×4	2.9271(8)	2.9225(17)	2.942(2)
Ni–O1 (Å)×2	2.027(4)	2.006(8)	2.028(6)
Ni–O2 (Å)×4	2.024(2)	2.002(2)	2.047(3)
Mo–O1 (Å)×2	1.919(4)	1.914(8)	1.923(6)
Mo–O2 (Å)×4	1.917(2)	1.940(3)	1.901(3)
wRp, Rp(%)	1.03,1.37	3.5,4.9[c]	4.49,3.46
χ^2	6.66	1.46[c]	2.31

Upon compression the tetragonal unit cell parameters (a_{tet} and c_{tet}) decrease with increasing pressure, and hence unit cell volume (V_{tet}) decreases, with no obvious discontinuities in their behaviour. Figure 2 shows the pseudo cubic lattice parameters ($a_{pc} = a_{tet}/\sqrt{2}$ and $c_{pc} = c_{tet}/2$) as a function of pressure. However, there is a difference in the rate of compression of the a_{tet} and c_{tet}-axes.

A 3^{rd} order Birch–Murnaghan equation–of–state (EoS) has been fitted to the data and the resulting fit is shown in Figure 2. The determined values are V_0=243.10(2) Å^3, B_0 =154.9(17) GPa and B'=3.1(6). The compressibilities of the a and c-axes are 2.13(1) and 1.71(2) TPa^{-1}, respectively. The bulk modulus is different to that determined previously (171(12) GPa) [16]. In the current study there are more data points to fit the EoS with, and there does not appear to be any peak broadening issues. Peak broadening was present in the previous study and was suggested to be attributed to stresses at grain–grain contacts and anti-phase boundaries, resulting from imperfect cation order. The value of the bulk modulus ∼ 155 GPa is comparable to other perovskite materials as de-

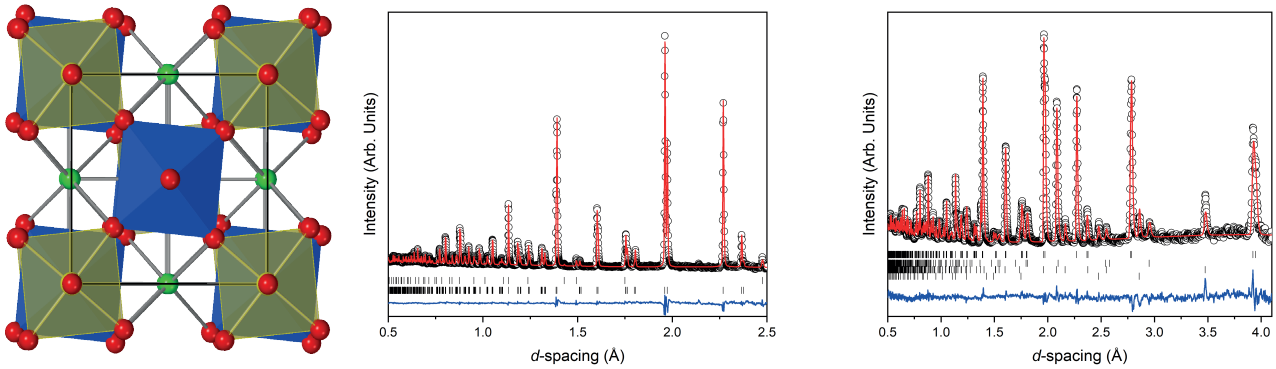

Figure 1: Left: Structure of Sr_2NiMoO_6 viewed down the c-axis. The NiO_6 octahedra are in blue and the MoO_6 octahedra in green. The red spheres show the oxygen atoms and the green spheres the strontium atoms. The black lines show the unit cell. The small tilting of the MoO_6 and NiO_6 octahedra of $\sim 7°$ is visible relative to the unit cell edge. Middle: Neutron powder diffraction pattern from the high resolution bank of the POLARIS instrument. The diffraction pattern measured is that from the recovered TiZr gasket, which still contains the Sr_2NiMoO_6 sample and the lead pellet. Right: Neutron powder diffraction pattern of Sr_2NiMoO_6 in the Paris–Edinburgh press at 0.08 GPa. In both panels the raw data are shown by the open black circles, the Rietveld fit by the solid red line, and the residual of the fit as the solid blue line. The vertical lines in the left panel show the reflection positions for the cubic lead (upper) and tetragonal Sr_2NiMoO_6 (lower). In the right panel the vertical blue lines show the reflection positions for (top to bottom) Sr_2NiMoO_6, Al_2O_3, ZrO_2 and Pb.

termined by *ab initio* modelling $B_0 = 143$ GPa for $SrMoO_3$ and experimentally for Sr_2CoMoO_6 B_0=152(9) GPa.[31, 32] The a/c ratio in Figure 2 shows a deviation away from the ideal value of 1 (where a sample would be metrically cubic) meaning that the sample is actually becoming more distorted (i.e. more tetragonal) with increasing pressure.

In the current work we see no measurable peak broadening across the entire diffraction pattern. At ~2.3 Å there appears to be a new reflection which appears in the diffraction pattern at a pressure of 4.5 GPa (see S.I.). This peak does not index as any suitable perovskite supercell or as any possible oxide contaminant, and we have made use of the recovered gasket to measure the diffraction pattern of the sample after compression and see no indication of the contaminant phase (Figure 1). One possibility is that it is a contaminant phase which is not readily visible at ambient pressure and potentially undergoes a phase transition to a symmetry which means that it is visible in the diffraction pattern. However, we do not rule out the possibility of it being form an incommensurate supercell but lack sufficient diffraction data to confirm this.

The response of materials to external stimuli (pressure or temperature) invariably results in some form of distortion or lattice relaxation on a macroscopic scale and gives rise to spontaneous strain.[33] The changes are a result of cooperative changes that occur on the microscopic scale. Hence, the lattice distortions represent the driving force for a transition. The determined magnitude of lattice strain (e) gives a measure of the extent of transformation at a given temperature or pressure. The spontaneous strains (Equation 1) are calculated from the difference between the pseudo–cubic tetragonal lattice parameters (a_{pc}, c_{pc}) and, in this case, a hypothetical cubic lattice parameter that would occur at the same temperature and pressure, divided by this hypothetical lattice parameter. At pressure there is no measured cubic behaviour to compare to, hence the expected cubic behaviour is determined from the cube root of the unit cell volume.

$$e_t(z) = \frac{2}{\sqrt{3}}\left(\frac{c_{pc}-a_{pc}}{a'}\right) \tag{1}$$

Figure 2 shows the variation in spontaneous strain with increasing pressure, showing a linear increase in distortion away from the cubic form, and hence no indication of approaching a phase transition.

A well established method of describing the distortion of the perovskite system is to parametrise the distortions in terms of the magnitudes of an appropriate set of symmetry-adapted basis-vectors of the primitive cubic aristotype phase at high-symmetry points of the Brillouin zone. [34] For $I4/m$ there are three active distortion modes: a breathing mode represented by *irrep* R_1^+ (d_1), a tilt mode represented by *irrep* R_4^+ (d_2) and a distortion mode represented by *irrep* R_3^+ (d_3). The amplitudes of the symmetry-adapted basis vectors (d_i) are related to the magnitudes of the structural distortions from ideality (r_j) via the matrix

$$\begin{bmatrix} d_1 \\ d_2 \\ d_3 \end{bmatrix} = \begin{bmatrix} -\frac{1}{3} & -\frac{1}{3} & -\frac{1}{3} \\ 0 & -\frac{1}{2} & \frac{1}{2} \\ \frac{1}{3} & -\frac{1}{6} & -\frac{1}{6} \end{bmatrix} \begin{bmatrix} r_1 \\ r_2 \\ r_3 \end{bmatrix} \tag{2}$$

where $r_1 = c_{tet}w_1, r_2 = \sqrt{2}a_{tet}u_2$ and $r_3 = \sqrt{2}a_{tet}v_2$.

Figure 3 shows the average and individual Mo-O and Ni-O bond lengths as a function of pressure, as determined by Rietveld analysis. Also shown is a linear fit to the bond lengths as determined by modal analysis. The Mo-O bond is more compressible than the Ni-O bond. This decrease in

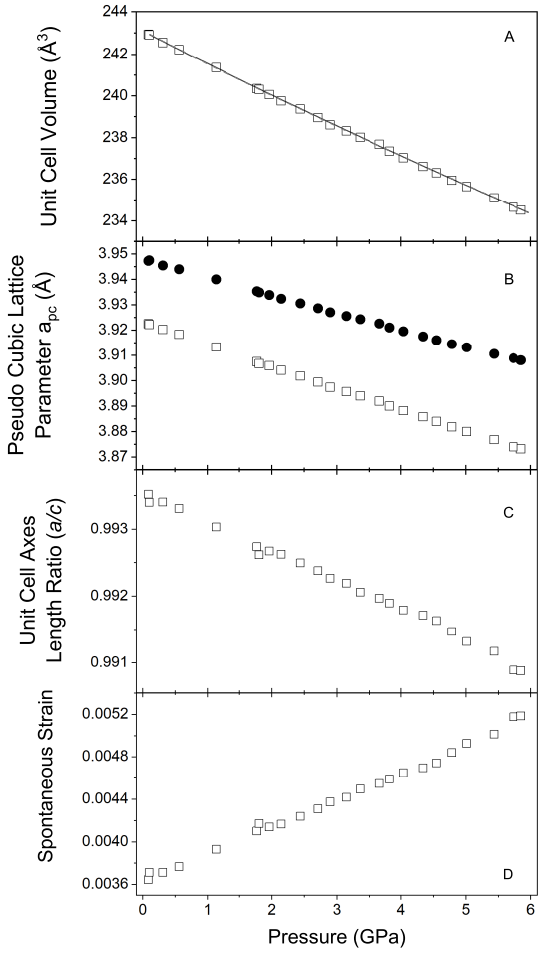

Figure 2: Variation in unit-cell parameters of Sr_2NiMoO_6 with increasing pressure. A: Unit cell volume (V_{tet}) experimental data shown as open squares. A 3rd order Birch-Murnaghan fit to the data is shown as black solid line. B: Pseudo cubic lattice parameters as a function of pressure $a_{pc} = b_{pc} = a_{tet}/\sqrt{2}$ (open squares), $c_{pc} = c_{tet}/2$ (filled circles). C: Unit cell axes ratio ($a_{tet}/(c_{tet}/\sqrt{2})$). D: Spontaneous strain ($e_t(z)$) as defined in main text. Where shown the errors are smaller than the symbols.

bond length is also reflected in the MoO_6/NiO_6 octahedra volume as shown in Figure 3. The distortion index (DI_{TO}) shows the distortion of the octahedra and as defined in equation 3 where n is the coordination number of the polyhedra, TO_i the individual bond length in the polyhedra and TO_m the average polyhedral bond length.[35] In both the NiO_6 and MoO_6 units the DI_{TO} does not change significantly with increasing pressure; this is also reflected in the change in the distortion mode d_3 which appears to be essentially zero (Figure 3).

$$DI_{TO} = \frac{1}{n}\left(\sum_{i=1}^{n} TO_i - TO_m\right) \quad (3)$$

The tilt angle ϕ of the octahedra can be calculated by [36]

$$\phi = arctan\left(2\sqrt[3]{\left(\frac{8}{V_{tet}}\right)}d_2\right) \quad (4)$$

Interestingly, the tilt angle (ϕ) of the octahedra increases further from that of the idealised cubic structure. This is again an indication of the increase in distortion of Sr_2NiMoO_6 overall with increasing pressure. The overall volume of the SrO_{12} polyhedra decreases with increasing pressure (Figure 4), but the distortion index (DI_{TO}) of the SrO_{12} polyhedra increases (Figure 4)— indicating a decrease in symmetry; this is driven by the rotation of the octahedra. This mechanism is also reflected in the compressibilities of each crystallographic axis with the *a* and *b*-axes being more compressible than the *c*-axis. The octahedra rotate around the *c*-axis and hence are mirrored in the compression of the *a* and *b*-axis whist the *c*-axis compresses by the decrease in bond lengths along the linear –O–M–O– chains formed by the corner sharing octahedra. The breathing mode (d_1) appears to be independent of pressure (Figure 3). We note that the data may suggest a correlated step change in behaviour of the polyhedra rotation and distortion around 4 GPa which could be an indication of a very subtle transition which would need to be isosymmetric and hence, first order in nature however, there is no indication of this in the variation of the unit–cell volume with pressure (see Figure 2).

It has previously been shown that the relative compressibilities of the octahedral (B) and distorted dodecahedral (A) cation sites in the perovskite structure can give an indication as to how the tilting of the octahedra will behave upon compression, either by increasing in tilt, tending towards lower symmetry, or a reduction in tilt and an increase in symmetry.[37] A model based upon the bond valence concept for each polyhedra has been developed that predicts the compressibility of the polyhedra.

The value M_i is the total estimated variation of bond valence in a polyhedral site due to the change of average bond distance and is defined as

$$M_i = \left(\frac{R_i N_i}{B}\right) exp\left[\left(\frac{R_0 - R_i}{B}\right)\right] \quad (5)$$

where R_i is the average measured bond distance in the polyhedra, N_i is the coordination number in the polyhedra, R_0 is a constant for a particular atom pair and B is a universal constant (0.37), the values of which are given and defined in ref [38]. The relative values of M for the A site (M_A) and (M_B) give an indication of the relative compressibilities (full derivation and description is given in ref [37]). For $M_A/M_B > 1$ the material will become more symmetric upon compression, $M_A/M_B \approx 1$ the distortion does not change with pressure and $M_A/M_B < 1$ indicates that the distortion will increase with increasing pressure.

At ambient pressure M_{Ni-O}=12.64 and M_{Mo-O}=28.76 and an average value for M_B of 20.70. In the dodecahedral SrO_{12} polyhedra there are four longer Sr–O bonds with an average value of 2.92 Å and eight shorter Sr–O bonds with an average value of 2.71 Å. As a result, and as described in

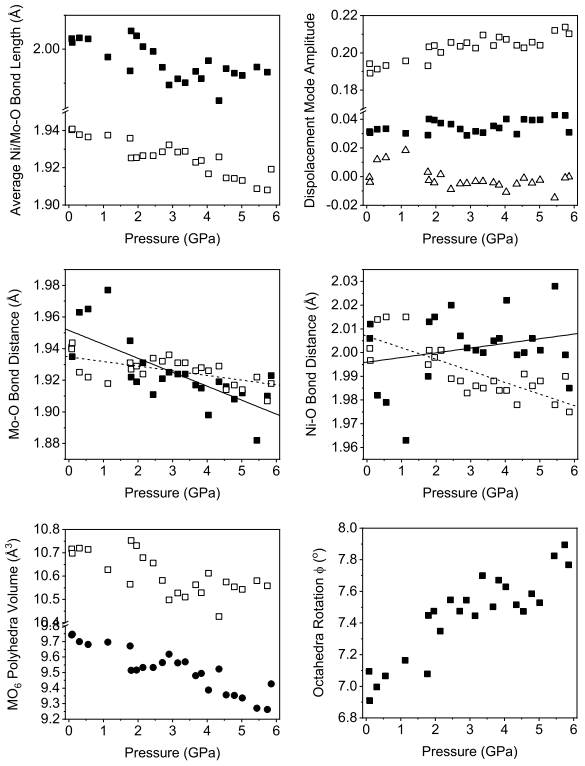

Figure 3: Polyhedra behaviour of Sr_2NiMoO_6 as a function of pressure. Top Left: Average Ni–O (solid squares) bond distance in MoO_6 (open squares) octahedra, as determined from Rietveld refinements. Top Right: Displacement mode amplitudes d_1—the breathing mode shown as solid squares, the tilt mode d_2 as the open squares and the distortion mode d_3 as open triangles. Middle Left: Mo-O bond lengths. The bond lengths determined from Rietveld analysis for Mo–O1 and Mo–O2 are shown as solid and open squares, respectively. The solid line shows a linear fit to the variation of the Mo–O1 bond lengths and the dashed line the Mo–O2 bond lengths, determined from displacement mode analysis. Middle Right: Ni–O bond lengths. The bond lengths determined from Rietveld analysis for Ni–O1 (solid squares) and Ni–O2 are shown as open squares. The solid line shows a linear fit to the variation of the Ni–O1 bond lengths, and the dashed line the Ni–O2 bond lengths determined from displacement mode analysis. Bottom Left: Variation in NiO_6 (open squares) and MoO_6 (filled circles) polyhedra volume. Bottom Right: MoO_6 and NiO_6 octahedral tilt (see equation 4).

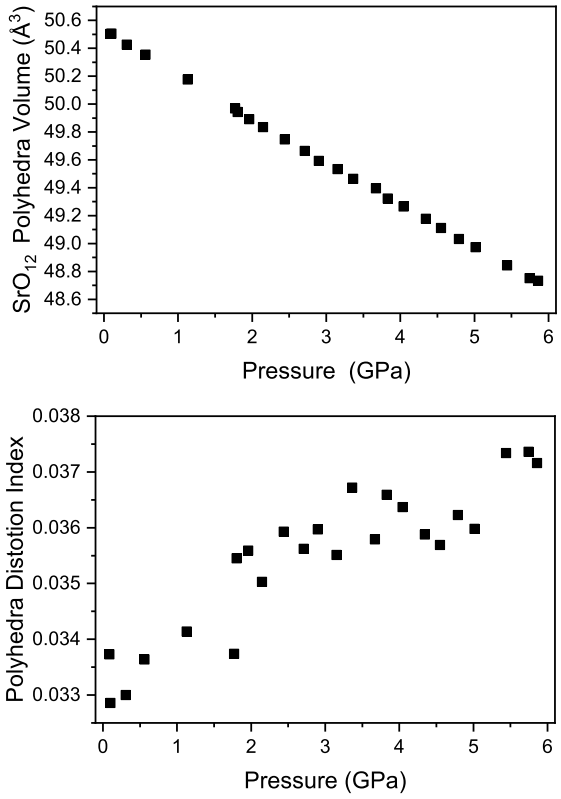

Figure 4: Behaviour of the SrO_{12} polyhedra as a function of pressure of Sr_2NiMoO_6. Top: SrO_{12} polyhedra volume. Bottom: SrO_{12} polyhedra distortion index as defined in equation 3.

the work of Zhao *et al*, the calculation is split into two parts for the determination of M_A and given by

$$M_{\mathrm{A}} = \left(8R_{\mathrm{S}}/B\right) exp\left(R_{\mathrm{S}}/B\right) + \left(4R_{\mathrm{L}}/B\right) exp\left(R_{\mathrm{L}}/B\right) \quad (6)$$

where R_S is the experimentally determined average shorter A–O bond lengths and R_L is the experimentally determined average longer A–O bond lengths in the SrO_{12} polyhedra. For Sr_2NiMoO_6 this gives a value of M_A of 15.34 and the ratio of $M_A/M_B \approx 0.74$. This suggests that the SrO_{12} polyhedra should be more compressible than the Ni/MoO_6 site. Hence, the structure will become more distorted and provides a reason for the increase in tetragonal distortion as is observed experimentally.

Figure 5 shows the variation in unit cell parameters of Sr_2NiMoO_6 with increasing temperature from 298–1400 K. In the tetragonal phase, the a and b-axes increase in length and the c-axis decreases in length, leading to an overall linear increase in unit cell volume. At 573 K there is a change in the diffraction pattern, where the non equivalent reflections (112 and 220) resulting from the tetragonal distortion, merge to form the single 220 reflection of the new cubic phase (Figure 5). This transition is in accordance with that previously reported. Figure 5 also shows the spontaneous strain of Sr_2NiMoO_6 as a function of temperature in the tetragonal phase according to equation 1, the pseudo-cubic lattice parameter (a') has been determined at each temperature below the transition by extrapolating the cubic lattice parameter behaviour back to 290 K. It can been seen that the strain approaches zero, linearly as it nears the phase transition.

In contrast to the previous high pressure studies [16] there appears to be no broadening of the diffraction peaks with increasing pressure. The peak broadening in the previous

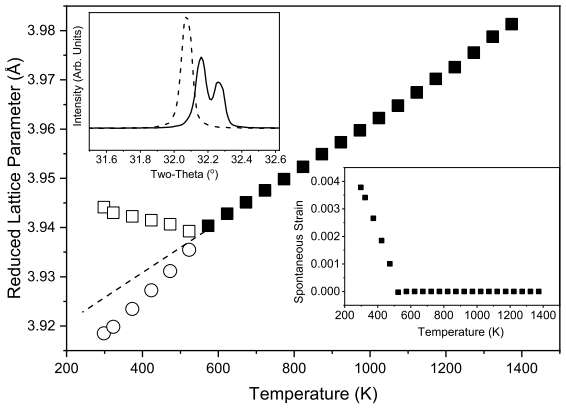

Figure 5: Variation in unit cell parameters of Sr_2NiMoO_6 with increasing temperature at ambient pressure. Where shown the errors are smaller than the symbols. The tetragonal a-axis (a_{tet}) is shown as open circles and the c-axis as the open squares. The solid squares are the lattice parameter for the cubic phase. The dashed line is the extrapolated cubic behaviour to lower temperature. The top inset shows the x-ray diffraction pattern at 298 K (solid line) of the tetragonal phase in the region of the 112 and 020 reflections and at 523 K (dashed line) of the cubic phase in the region of the 220 reflection. The bottom inset shows the change in spontaneous strain $e_t(z)$ determined from the x-ray data diffraction data.

study was suggested to be a result of grain–grain contacts and anti-phase boundaries resulting from imperfect cation order. It was reported that in the broadened peaks a phase transition to monoclinic symmetry with the space group $P2_1/n$ could have occurred but could find no definitive evidence for this beyond peak broadening and may well be a result of the low resolution of the study. In particular it was suggested that the region around the 024/132 reflections at ∼1.6 Å would split into the $204/20\bar{4}/132/13\bar{2}$ reflections if the sample became monoclinic and, the 224/040 reflections would split to form the $22\bar{4}/224/040/400$ reflections at ∼ 1.39 Å. No such peak broadening or splitting is observed in these regions in the diffraction pattern across the whole pressure range studied. We suggest that the previous study was adversely affected by compression in non-hydrostatic conditions.

4. Conclusions

The high-pressure behaviour of Sr_2NiMoO_6 has been followed using neutron powder diffraction. We have shown how the sample compresses and becomes less symmetric as the pressure increases. The compression behaviour is found to occur by a concerted rotation of the MoO_6 and NiO_6 around the c-axis. The fact that Sr_2NiMO_6 decreases in symmetry at high pressure can be understood by the difference in compressibilties of the Ni and Mo octahedra relative to the SrO_{12} polyhedra.

5. Acknowledgements

The authors wist to thanks STFC for access to the ISIS neutron and muon facility.[39] Ron Smith for help in collecting data on the POLARIS instrument, We also acknowledge the help of Daniel Nye and Gavin Stenning of the MCL at the ISIS Neutron and Muon Facility.

6. Bibliography

References

[1] M. T. Anderson, K. B. Greenwood, G. A. Taylor, K. R. Poeppelmeier, B-cation arrangements in double perovskites, Progress in Solid State Chemistry 22 (1993) 197 – 233.

[2] P. W. Barnes, M. W. Lufaso, P. M. Woodward, Structure determination of $A_2M^{3+}TaO_6$ and $A_2M^{3+}NbO_6$ ordered perovskites: octahedral tilting and pseudosymmetry, Acta Crystallographica Section B 62 (2006) 384–396.

[3] A. Azad, S. Ivanov, S. G. Eriksson, J. Eriksen, H. Rundlöf, R. Mathieu, P. Svedlindh, Synthesis, crystal structure, and magnetic characterization of the double perovskite Ba_2MnWO_6, Materials Research Bulletin 36 (2001) 2215 – 2228.

[4] G. Chen, C. Dai, C. Ma, A stable half-metallic ferromagnetic material $SrNiO_3$: a prediction from first principles, in: 2014 International Conference on Mechatronics, Electronic, Industrial and Control Engineering (MEIC-14), Atlantis Press, 2014/11. URL: https://doi.org/10.2991/meic-14.2014.167. doi:https://doi.org/10.2991/meic-14.2014.167.

[5] I. C. Lekshmi, A. Gayen, M. Hegde, The effect of strain on nonlinear temperature dependence of resistivity in $SrMoO_3$ and $SrMoO_{3-x}N_x$ films, Materials Research Bulletin 40 (2005) 93 – 104.

[6] L. Brixner, X-ray study and electrical properties of system $Ba_xSr_{(1-x)}MoO_3$, Journal of Inorganic and Nuclear Chemistry 14 (1960) 225 – 230.

[7] H. Mizoguchi, K. Fukumi, N. Kitamura, T. Takeuchi, J. Hayakawa, H. Yamanaka, H. Yanagi, H. Hosono, H. Kawazoe, Electronic structure of polycrystalline $AMoO_3$ (A=Sr or Ba), Journal of Applied Physics 85 (1999) 6502–6505.

[8] A. M. Glazer, The classification of tilted octahedra in perovskites, Acta Crystallographica Section B 28 (1972) 3384–3392.

[9] A. K. Eriksson, S. G. Eriksson, S. Ivanov, C. Knee, J. Eriksen, H. Rundlöf, M. Tseggai, High temperature phase transition of the magnetoelectric double perovskite Sr_2NiMoO_6 by neutron diffraction, Materials Research Bulletin 41 (2006) 144 – 157.

[10] L. H. Brixner, Preparation and structure determination of some new cubic and tetragonally-distorted perovskites, The Journal of Physical Chemistry 64 (1960) 165–166.

[11] S. Nomura, T. Nakagawa, Structural and magnetic transitions in $Sr_2(NiMo)\ O_6$, Journal of the Physical Society of Japan 21 (1966) 1068–1071.

[12] V. V. Gagulin, S. K. Korchagina, V. V. Ivanova, Y. A. Shevchuk, Synthesis and properties of Sr_2CoMoO_6 and Sr_2NiMoO_6, Inorganic Materials 39 (2003) 625–626.

[13] Y. Teraoka, M. Wei, S. Kagawa, Double perovskites containing hexavalent molybdenum and tungsten: synthesis, structural investigation and proposal of a fitness factor to discriminate the crystal symmetry, J. Mater. Chem. 8 (1998) 2323–2325.

[14] M. Martínez-Lope, J. Alonso, M. Casais, Synthesis, crystal and magnetic structure of the double perovskites A_2NiMoO_6(A = Sr, Ba): a neutron diffraction study, European Journal of Inorganic Chemistry 2003 (2003) 2839–2844.

[15] V. G. Gunjikar, N. Ramachandran, K. H. V, Heat-capacity and thermodynamic properties of Sr_2MoCoO_6 and Sr_2MoNiO_6, J. Indian Chem. Soc. 59 (1982) 743–744.

[16] M. W. Lufaso, R. B. Macquart, Y. Lee, T. Vogt, H.-C. zur Loye, Structural studies of Sr_2GaSbO_6, Sr_2NiMoO_6, and Sr_2FeNbO_6 us-

ing pressure and temperature, Journal of Physics: Condensed Matter 18 (2006) 8761–8780.
[17] E. Ksepko, Perovskite-type $Sr(Mn_{1-x}Ni_x)O_3$ materials and their chemical-looping oxygen transfer properties, International Journal of Hydrogen Energy 39 (2014) 8126 – 8137.
[18] M. Zinkevich, Constitution of the Sr–Ni–O system, Journal of Solid State Chemistry 178 (2005) 2818 – 2824.
[19] C. J. Ridley, D. Daisenberger, C. W. Wilson, G. B. G. Stenning, G. Sankar, K. S. Knight, M. G. Tucker, R. I. Smith, C. L. Bull, High-pressure study of the elpasolite perovskite La_2NiMnO_6, Inorganic Chemistry 58 (2019) 9016–9027. PMID: 31241907.
[20] J. S. Olsen, L. Gerward, G. Vaitheeswaran, V. Kanchana, L. Alff, High-pressure structural behavior of the double perovskite Sr_2CrReO_6: an experimental and theoretical study, High Pressure Research 29 (2009) 83–86.
[21] L. S. I. Veiga, G. Fabbris, M. van Veenendaal, N. M. Souza-Neto, H. L. Feng, K. Yamaura, D. Haskel, Fragility of ferromagnetic double exchange interactions and pressure tuning of magnetism in $3d-5d$ double perovskite Sr_2FeOsO_6, Phys. Rev. B 91 (2015) 235135.
[22] V. V. Sereda, D. S. Tsvetkov, A. L. Sednev, A. I. Druzhinina, D. A. Malyshkin, A. Y. Zuev, Thermodynamics of Sr_2NiMoO_6 and Sr_2CoMoO_6 and their stability under reducing conditions, Phys. Chem. Chem. Phys. 20 (2018) 20108–20116.
[23] R. I. Smith, S. Hull, M. G. Tucker, H. Y. Playford, D. J. McPhail, S. P. Waller, S. T. Norberg, The upgraded Polaris powder diffractometer at the ISIS neutron source, Review of Scientific Instruments 90 (2019) 115101.
[24] C. L. Bull, N. P. Funnell, M. G. Tucker, S. Hull, D. J. Francis, W. G. Marshall, PEARL: the high pressure neutron powder diffractometer at ISIS, High Pressure Research 36 (2016) 493–511.
[25] W. G. Marshall, D. J. Francis, Attainment of near-hydrostatic compression conditions using the Paris-Edinburgh cell, J. Appl. Crystallogr. 35 (2002) 122–125.
[26] S. Klotz, J. C. Chervin, P. Munsch, G. L. Marchand, Hydrostatic limits of 11 pressure transmitting media, J. Phys. D: Appl. Phys. 42 (2009) 075413.
[27] J. M. Besson, R. J. Nelmes, G. Hamel, J. S. Loveday, G. Weill, S. Hull, Neutron powder diffraction above 10 GPa, Physica B 180 (1992) 907–910.
[28] O. Arnold, J. C. Bilheux, J. M. Borreguero, A. Buts, S. I. Campbell, L. Chapon, M. Doucet, N. Draper, R. Ferraz Leal, M. A. Gigg, V. E. Lynch, A. Markvardsen, D. J. Mikkelson, R. L. Mikkelson, R. Miller, K. Palmen, P. Parker, G. Passos, T. G. Perring, P. F. Peterson, S. Ren, M. A. Reuter, A. T. Savici, J. W. Taylor, R. J. Taylor, R. Tolchenov, W. Zhou, J. Zikovsky, Mantid—Data analysis and visualization package for neutron scattering and μSR experiments, Nucl. Instrum. Meth. A 764 (2014) 156–166.
[29] B. H. Toby, *EXPGUI*, a graphical user interface for *GSAS*, J. Appl. Crystallogr. 34 (2001) 210–213.
[30] M. J. Cliffe, A. L. Goodwin, *PASCal*: a principal axis strain calculator for thermal expansion and compressibility determination, Journal of Applied Crystallography 45 (2012) 1321–1329.
[31] A. Daga, S. Sharma, Ab–initio Structural Study of $SrMoO_3$, Journal of Modern Physics 3 (2012) 1891–1894.
[32] M. W. Lufaso, W. R. Gemmill, S. J. Mugavero, Y. Lee, T. Vogt, H. zur Loye, Compression mechanisms of symmetric and Jahn–Teller distorted octahedra in double perovskites: A_2CuWO_6 (A=Sr, Ba), Sr_2CoMoO_6, and La_2LiRuO_6, Journal of Solid State Chemistry 179 (2006) 3556 – 3561.
[33] M. A. Carpenter, E. K. Salje, A. Graeme-Barber, Spontaneous strain as a determinant of thermodynamic properties for phase transitions in minerals, European Journal of Mineralogy 10 (1998) 621–691.
[34] K. S. Knight, Parameterization of centrosymmetric elpasolite-type crystal structures in terms of symmetry-adapted basis-vectors of the primitive cubic aristotype phase, The Canadian Mineralogist 47 (2009) 401–420.
[35] W. H. Baur, The geometry of polyhedral distortions. Predictive relationships for the phosphate group, Acta Crystallographica Section B 30 (1974) 1195–1215.
[36] K. S. Knight, Parameterization of the crystal structures of centrosymmetric zone-boundary-tilted perovskites: an analysis in terms of symmetry-adapted basis-vectors of the cubic aristotype phase, The Canadian Mineralogist 47 (2009) 381–400.
[37] J. Zhao, N. L. Ross, R. J. Angel, New view of the high-pressure behaviour of $GdFeO_3$-type perovskites, Acta Crystallographica Section B 60 (2004) 263–271.
[38] I. D. Brown, D. Altermatt, Bond-valence parameters obtained from a systematic analysis of the Inorganic Crystal Structure Database, Acta Crystallographica Section B 41 (1985) 244–247.
[39] C. L. Bull, C. J. Ridley, N. P. Funnell, 10.5286/ISIS.E.RB1820172 (2019).